Analysis of Near Field Spatio-Temporal Sound Wave Radiation from Finite Aperture Piezoelectric Transducer

Akira YAMADA*, and Yoshio UDAGAWA[1] †

Graduate School of Bio-Applications and Systems Engineering,Tokyo University of Agriculture and Technology, Koganei, Tokyo 184-8588, Japan

[1]*Imaging Supersonic Laboratories Co.Ltd., Nara, Nara , Japan*

Physical behavior of the near field spatio-temporal sound wave radiation from a finite aperture piezoelectric transducer was investigated in detail. Simulation analysis was made using finite difference time domain (FDTD) method choosing displacement as an independent variable. Mechanism of transient radiation wave field behavior from the finite aperture transducer was clarified. The results of comparative examination between simulation and photo elastic imaging experiment showed the validity of our clarification.

1. Introduction

Theoretical analysis of spatio-temporal radiation sound field in a medium by finite aperture piezoelectric plate is important for the design of ultrasound transducers in nondestructive testing[1,2] and/or medical imaging.[3–5] Waves emitted from the plate edge in addition to a primary plane wave make it difficult to understand the behavior of spatio-temporal variation of the radiated sound field. There are many studies based on the Rayleigh integral formula,[6–11] integral transform technique,[12] and finite difference time domain (FDTD) numerical simulation[13] etc. It might be considered as a resolved problem, however, reports are very few showing agreement between theory and experiment, especially in near spatio-temporal radiation field. For instance, method using conventional Rayleigh integral formula have questions on the points: (i) inappropriate spatial boundary condition such as rigid baffle assumption around vibrating plate as well as abrupt discontinuous displacement at the peripheral border of vibrator, (ii) inappropriate excitation condition which is different from actual experimental set-up, (iii) generation of contour mode vibration other than primary longitudinal thickness mode vibration, (iv) discrepancy between frequency and time domain analysis.

*E-mail address: yamada@cc.tuat.ac.jp
†E-mail address: isl@kcn.ne.jp

As a rule, FDTD method[14–16] is expected to encounter the problems described above, since the method is based on the rigorous time domain calculation of the wave equation. In this situation, however, it must be in accordance with an actual high voltage pulser, where the vibrator is excited by short period discontinuous signal like step or impulse voltage signal,[13,18] rather than usual pulsed sine signal.

Taking these into considerations, time domain response of the vibrator under the step voltage excitation is strictly considered as initial excitation condition of the displacement at the vibrator surface. Numerical FDTD simulations are made choosing displacement as an independent variable. Spatio-temporal radiation field in the vicinity of the plate edge is investigated in detail. As a result, mechanism of transient radiation field behavior from the finite aperture transducer is clarified. At the end of the paper, numerical results are compared with photo-elastic sound field visualization[13,19,20] experiments. The comparative examination between simulation and experiment shows the validity of our clarification.

2. Temporal response of vibrator by transient excitation

2.1 Step voltage excitation

A piezoelectric vibrator plate with thickness l is considered as shown in Fig. 1. The vibrator plate is attached to a semi-infinite target medium and backed with a semi-infinite sound absorbing material. Sufficiently thin metallic electrodes are attached on the front and back surface of the plate. As mentioned above, the vibrator plate is excited with step voltage time function as shown in Fig.2(a). One dimensional longitudinal plane wave propagation in x-directions then assumed, that is to say, fields in transverse y direction are assumed to be uniform. The condition is satisfied when aperture width of the vibrator is much larger than thickness l. Current I across the electrodes is related with the applied voltage V as

$$I = C\frac{dV}{dt}. \tag{1}$$

where C is electrostatic capacitance between electrodes. By substituting a step voltage function into eq.(1), we can see that induced current I becomes impulse as shown in Fig.2(b).

2.2 Evolution of unipolar rectangle stress wave

We will now show the evolution of unipolar rectangle shaped stress wave propagating toward the medium. First, caused by the impulse current, stress T_0 with uniform

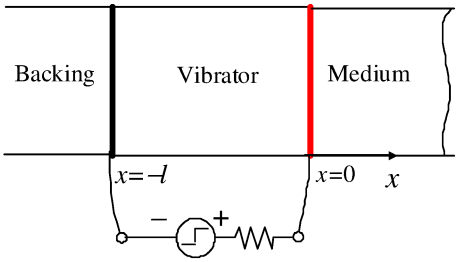

Fig. 1. Geometry of piezoelectric vibrator plate.

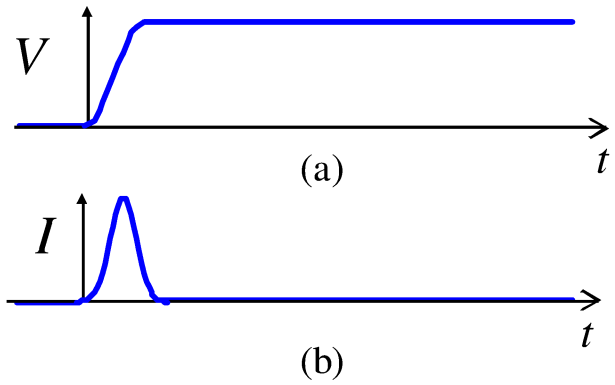

Fig. 2. Excitation waveform of (a)voltage V and (b) current I.

rectangular shape distribution as shown in Fig.3 (a) is instantaneously induced in the vibrator. Next, external forces F^+ ans F^- are operated at the edges of T_0 which are proportional to gradient of T_0. Excited by the external forces, stress waves $T^+(x-ct)$ and $T^-(x+ct)$ then begin to propagate forward x^+ and backward x^- directions with sound speed c, as shown in Fig.3 (b). As time advances ($t > 0$), they propagate toward opposite $x^\pm$ directions. They eventually separate into two rectangular waves as shown in Fig.3 (c). Immediately after separation, external forces disappear. Note that under complete backing condition, backward wave toward $-x$ direction is absorbed. Finally, unipolar rectangle stress wave $T^+(x-ct)$ with duration l/c is emitted toward the target medium from front surface of the vibrator as shown in Fig.3 (d).

2.3 Temporal variation of stress wave and displacement

So far, spatial variations along x-axis was considered. Temporal variation with respect to time t is considered as well. That is, fixing spatial position at $x = 0$, temporal variation of stress is obtained as the wave passing through the position $x = 0$ with sound speed c. Therefore, time dependency of the stress $T^+(t)$ becomes as shown in

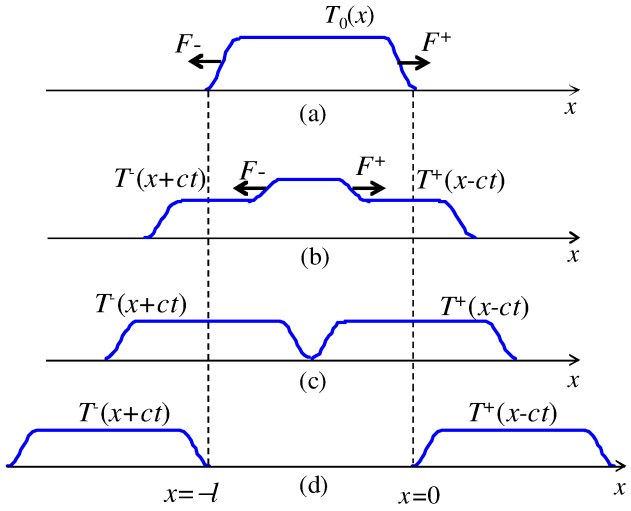

Fig. 3. Schematic to illustrate the generation of rectangle shaped stress wave.

Fig.4(a).

2.4 Unilateral trapezoidal displacement in front of the vibrator surface

Normal stress T_{xx} and displacement u_x in the direction x are related with following equation:

$$T_{xx}(x-ct) = \rho c^2 \frac{du_x(x-ct)}{dx} \tag{2}$$

Displacement u_x is, therefore, obtained by spatial integral of stress T_{xx}.

$$u_x(x-ct) = \frac{1}{\rho c^2} \int T_{xx}(x-ct)dx \tag{3}$$

Assuming rectangular shaped function for T_{xx}, it follows that displacement u with unilateral trapezoidal step function as shown in Fig. 4(b) is obtained.

2.5 Wave equation of elastic waves in the target medium

Displacement u of the waves in the target solid medium are governed by the following wave equation.

$$\begin{aligned} (\lambda+2\mu)\frac{\partial^2 u_x}{\partial x^2} + \mu\frac{\partial^2 u_x}{\partial y^2} + (\lambda+\mu)\frac{\partial^2 u_y}{\partial x \partial y} - \rho\frac{\partial^2 u_x}{\partial t^2} &= -f_x \\ (\lambda+2\mu)\frac{\partial^2 u_y}{\partial y^2} + \mu\frac{\partial^2 u_y}{\partial x^2} + (\lambda+\mu)\frac{\partial^2 u_x}{\partial x \partial y} - \rho\frac{\partial^2 u_y}{\partial t^2} &= -f_y \end{aligned} \tag{4}$$

where λ and μ are Lamé's constant in the medium and f_x and f_y are external forces in x and y direction, respectively. Equation (4) is a basic wave equation selecting displacement u as independent variable. Once, displacements u is determined in the

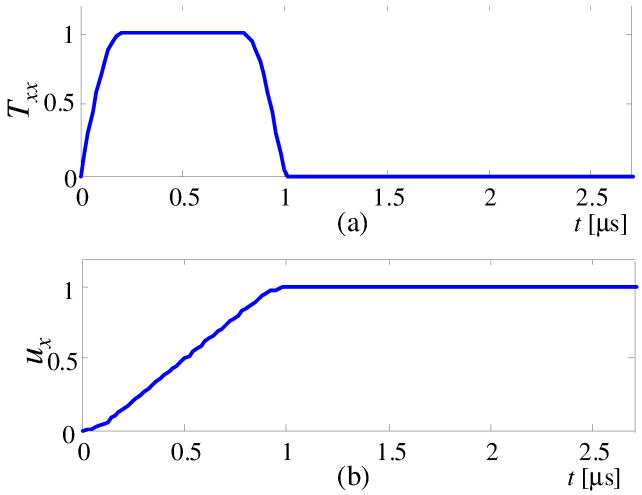

Fig. 4. Temporal waveform at the vibrator surface, (a)normal stress $T_{xx}(t)$, (b)displacement u_x.

FDTD calculations, stress is obtained from the derivative of displacement as follows:

$$\begin{aligned} T_{xx} &= (\lambda + 2\mu)\frac{\partial u_x}{\partial x} + \lambda\frac{\partial u_y}{\partial y} \\ T_{yy} &= (\lambda + 2\mu)\frac{\partial u_y}{\partial y} + \lambda\frac{\partial u_x}{\partial x} \\ T_{xy} &= \frac{\mu}{2}\left(\frac{\partial u_x}{\partial y} + \frac{\partial u_y}{\partial x}\right) \end{aligned} \tag{5}$$

Similarly, remaining quantities are obtained from the spatial or temporal derivative of u as well. It is noted that there is no need for integral calculation which makes it possible to be handled much easier and realize accurate calculation. For this reason, FDTD calculations are made below based on the equations choosing displacements u as independent variables.

3. Numerical simulation

3.1 Method

In 2D (x, y) coordinate, piezoelectric vibrator with aperture semi-infinite width is placed, edge of which is adjusted to the origin of y-axis as shown in Fig. 5. We consider simulation calculations for the sound wave field radiated in the semi-infinite half space $x > 0$ when the vibrator is excited by transient step voltage. Here, we used the 2D FDTD simulation software Wave2000◯(Cyber Logic),[14] which calculates wave field using displacement as independent variable. A vibrator with center frequency f_0=500 kHz was considered. Material parameters of the solid medium were set assuming borosilicate glass with density $\rho = 2320$ kg/m^3, Lamé's constant λ=23,879 MPa, and μ=24,959 MPa, (longitudinal wave sound speed c_l=5,640 m/s, shear wave sound speed c_s=3,280 m/s). As described in previous section, time dependence of initial vibrator surface dis-

placement was set with unilateral trapezoidal function beginning at time t=0 with rising edge width $t = 1.0\mu s$ (Fig. 4(b)) Where, for stabilization of solution, edges of the unilateral trapezoidal function are rounded. Corresponding normal stress T_{xx} is as shown in Fig. 4(a), which is derived from the differential calculation of displacement.

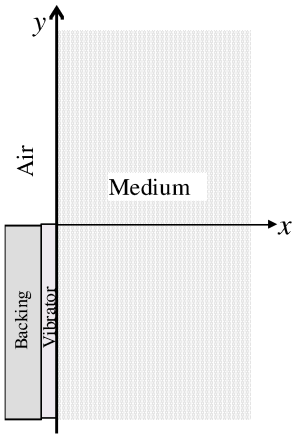

Fig. 5. Geometry for a vibrator plate, radiating into semi-infinite solid medium.

3.2 Simulation result of displacement field

Simulated displacement field in the vicinity of a vibrator edge at a time $t = 4.3$ μs was calculated as shown in Fig. 6, where (a) and (b) is gray scale images of displacement u_x in x and u_y in y directions, respectively and (c) is a vector diagram of displacement. We can see that, primary longitudinal plane wave (P wave) is emitted from the vibrator surface (Fig. 6(a)). In addition, rotational displacements (green lines in Fig. 6(c)) are generated around edge point toward the exterior direction). Cause of the rotational displacement is considered as follows. At the rising edge of the trapezoidal excitation, pushing displacement is generated toward exterior direction. As described below, longitudinal edge stress wave called BED (Beam Edge Diffusion) wave as well as shear edge stress wave are excited driven by the rotational displacement.

3.3 Simulation result of stress wave field

From the spatial derivative calculation of displacement according to eq.(5), normal stress T_{xx} and T_{yy} as well as shear stress T_{xy} were obtained as shown in Fig. 7. The sectional slices of the normal stress T_{xx} along x- and y-direction are shown in Fig. 7(a) and (b), respectively. We can see that flat amplitude rectangular shaped longitudinal plane wave is propagating from the vibrator surface. In addition, BED having cylindrical

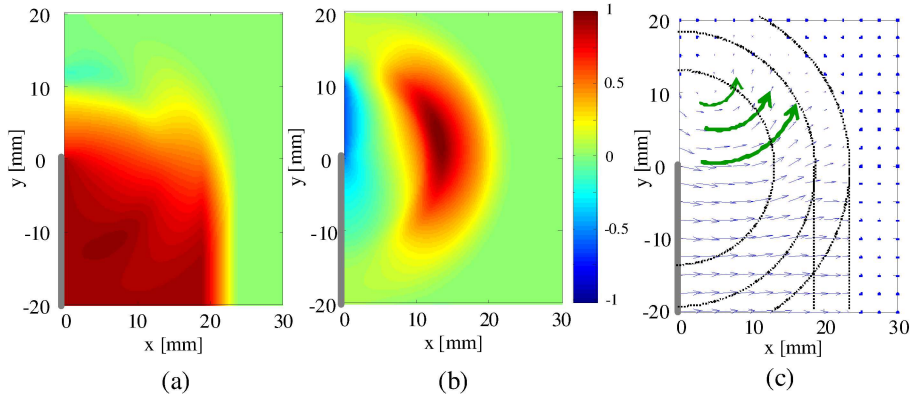

Fig. 6. Simulation result of displacement field for $t = 4.3\mu s$, (a) gray scale image of (a)u_x, and (b)u_y, (c) vector diagram of displacement.

longitudinal wave emanating from the edge with longitudinal sound speed propagate, they are superposed to the primary plane wave field. Note that exterior BED stress field has positive sign, on the other hand, interior part has negative. We can also recognize that shear edge wave propagates having similar cylindrical wave-front with shear wave speed. At the inter-medium region between the crest of longitudinal (P wave and BED) and shear wave, residual stress wave field can be seen driven by the of peripheral displacement. The behavior of these radiation waves are schematically illustrated as shown in Fig. 8.

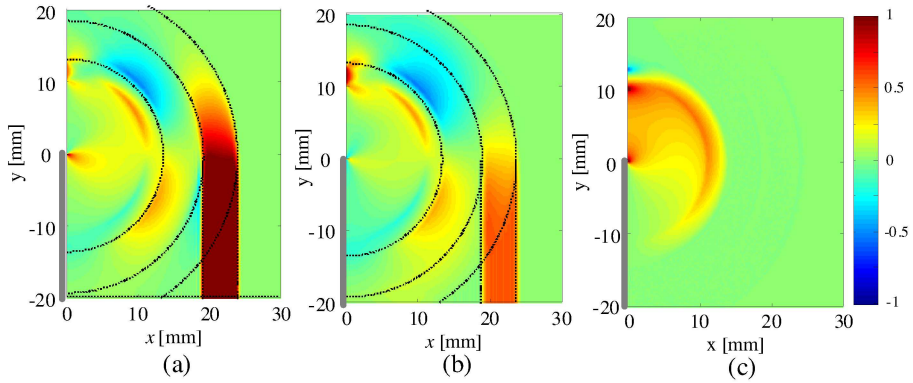

Fig. 7. Simulation result of stress field for $t = 4.3\mu s$, gray scale image of (a)T_{xx} and (b)T_{yy}, (c) T_{xy}.

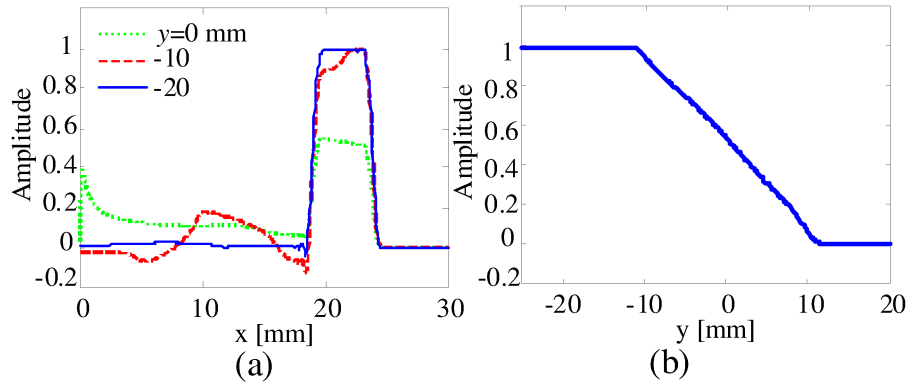

Fig. 8. Simulation result of stress field for $t = 4.3\mu s$, cross sectional profile along (a)x direction, (b)y direction at the center of the plane longitudinal wave.

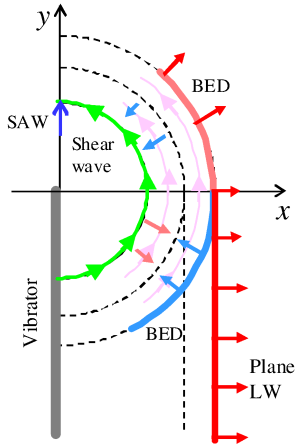

Fig. 9. Schematics of radiation wave fields.

4. Photo-elastic visualization experiment

4.1 Experiment set-up

Photo-elastic sound wave visualization system[13,19,20] prepared in our laboratory was as shown in Fig. 9. The system consists of a stroboscopic light source, a pair of linear polarizer plates, collimating and viewing lenses, and CCD cameras. Piezoelectric vibrator plate (center frequency 0.5 MHz, circular with diameter 40 mm) was attached to the borosilicate glass test piece ($W \times D \times H$: $40 \times 15 \times 40mm$) as shown in Fig. 10. Ultrasound waves were excited by step pulser (ISL, step voltage 1000V, charge current width 100 ns). Light was emitted from the stroboscopic source, after polarized with a polarizer, illuminated the glass piece from the direction normal to the sound wave propagation direction. Output light was detected by an analyzing polarizer. Polarization angle between input and output polarizer was maintained with 90 degree. It is

known that output light intensity I is proportional to the difference of the orthogonal principal stress $\sigma_1 - \sigma_2$ in the medium as,

$$I = a^2 \sin^2\theta \sin^2\{CD(\sigma_1 - \sigma_2)\} \tag{6}$$

where a is a coefficient, θ is an angle between polarization direction and sound propagation direction, C and D are photo-elastic constant and thickness of the test piece. Note that intensity of light becomes maximum when $\theta = \pi/4$ for the difference between x and y orthogonal principal stress (longitudinal wave component), on the other hand, when $\theta = 0$ for diagonal directional principal stress (normal stresses in 45 degree rotated coordinate axis). In the former case, longitudinal wave component can be detected, on the other hand, in the latter case, transverse wave component. By using a imaging lens, normal stress difference field image was finally formed over a CCD camera. When a delay of light emission with respect to the sound wave excitation was adjusted to time t, frozen image at a time when the sound wave propagated at distance $L = ct$ was visualized.

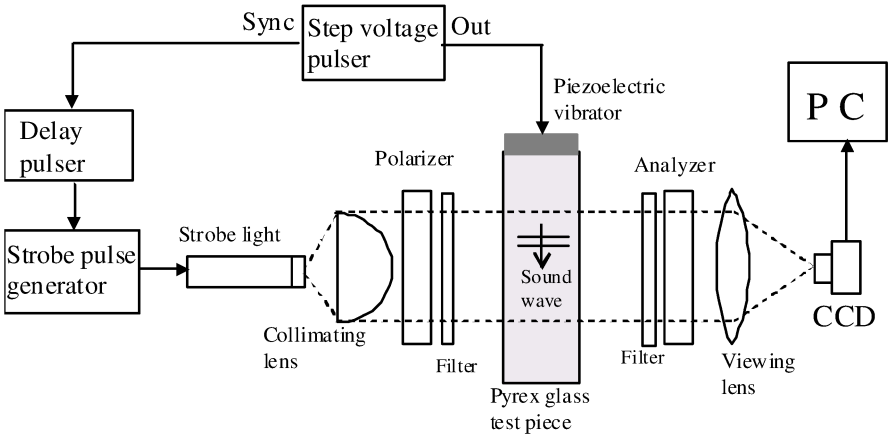

Fig. 10. Photo-elastic sound radiation field visualization system.

4.2 Results

Observation was made using photo-elastic visualization experiment apparatus. Piezoelectric circular plate was attached on the top surface of the test glass piece. Plate was placed over the glass surface as shown in Fig 10., at the position so that edge of the plate to be coincident with center of the glass surface. Assuming that thickness D of the test piece was small compared to width W, radiated sound field was regarded as 2 dimensional. The plate was backed with same piezoelectric material, so that returning

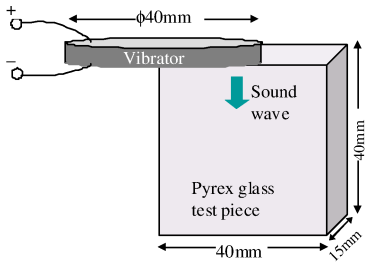

Fig. 11. Arrangement of the piezoelectric vibrator plate and test piece.

backward wave was suppressed. Step voltage was applied to the vibrator plate. Measured photo-elastic image of radiated sound field at time $t = 4.3\mu s$ is shown in Fig. 11, where (a) is the image measured choosing polarization angle $\theta = 45°$, (b) is the image for $\theta = 0°$. Corresponding simulation image is also compared as shown in Fig. 12, where (a) is the image of difference of normal stress $T_{xx} - T_{yy}$ and (b) is $T_{x'x'} - T_{y'y'}$ in 45 degree rotated x' and y' direction. It can be seen that sound propagations of primary plane longitudinal wave, BED, and shear wave are clearly visible. They show very close appearance between simulation and experiment.

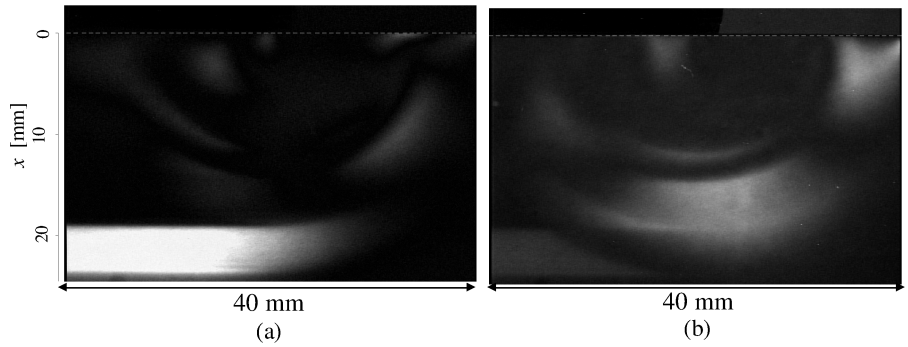

Fig. 12. Experimental results of photo-elastic images at time $t = 4.3\mu s$, (a) image measured with polarization angle $\theta = 45°$, (b) image with $\theta = 0°$.

5. Conclusions

Spatio-temporal characteristics of radiation sound field was elucidated based on the FDTD numerical simulations. It was demonstrated that results of simulations were in excellent agreement with photo-elastic sound field visualization experiment. On the whole, temporal domain sound wave radiation phenomena from finite aperture vibrator was clarified which agrees well with experiment. It should be noted that in the medium with high attenuation, agreement between theory and experiment becomes much worse.

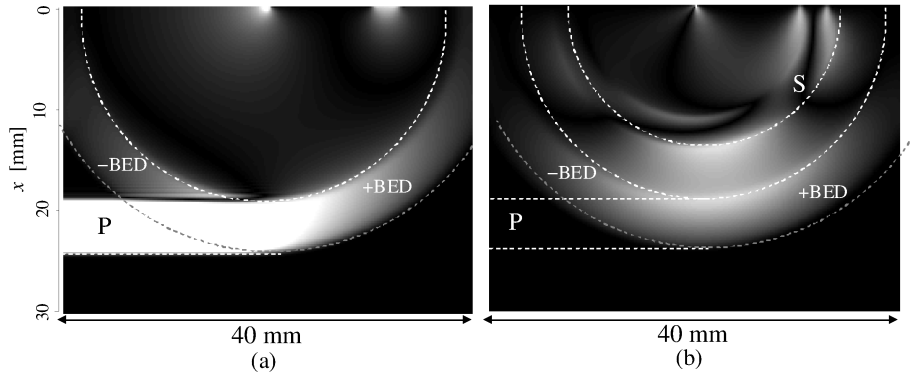

Fig. 13. Simulated results corresponding to the image shown in Fig.12, (a)normal stress difference $T_{xx} - T_{yy}$ along x and y direction and (b) $T_{x'x'} - T_{y'y'}$ along 45 degree rotated x' and y' direction.

The issue is beyond the scope of this paper, therefore, remained as our future work .

References

1) M. Fukuda and K. Imano,: Jpn. J. Appl. Phys. **51** (2012) 07GB06.
2) M. Ikeuchi, K. Jinno, Y. Ohara, and K. Yamanaka: Jpn. J. Appl. Phys. **52** (2013) 07HC08.
3) I. Akiyama, N. Yoshizumi, S. Saito, Y. Wada, D. Koyama, and K. Nakamura: Jpn. J. Appl. Phys. **51** (2012) 07GF02.
4) R. Narumi, K. Matsuki, S. Mitarai, T. Azuma, K. Okita, A. Sasaki, K. Yoshinaka, S. Takagi, and Y. Matsumoto: Jpn. J. Appl. Phys. **52** (2013) 07HF01.
5) A. Asai, H. Okano, S. Yoshizawa, and S. Umemura: Jpn. J. Appl. Phys. **52** (2013) 07HF02.
6) P. R. Stepanishen: J.Acoust.Soc.Am.,**49**,(1971)841.
7) G. R. Harris: J.Acoust.Soc.Am.**70** (1981) 10.
8) J. A. Jensen and N.B.Svendsen :IEEE Trans. Ultrason. Ferroelectr. Freq. Control.**39**(1992)262.
9) J. A. Jensen: 10th Nordic-Baltic Conf. on Biomedical Imaging,1996,p. 351.
10) T. Otani: *Handbook of Ultrasound, section 2-3* [in Japanese], (Nikkan Kogyo Shimbun, Tokyo 2010).
11) J. F. Kelly and R. J. McGough:IEEE Trans. Ultrason. Ferroelectr. Freq. Control. **53** (2006) 1150.
12) H. Dielouah and J. C. Baboux: J.Acoust.Soc.Am. **92**(1992)2932.
13) Y. Udagawa: *Introduction to Ultrasonic Wave Technique - Transducer, Pulser, Receiver and Device-* (Nikkan Kogyo Shimbun, Tokyo 2010).
14) R.S.Schechter, H.H.Chaskelis, R.B.Mignogna, P.P.Delsanto: Science, **265** (1994)1188.
15) Y. Miyazaki and T. Tsuchiya: Jpn. J. Appl. Phys. **51** (2012) 07GB02.
16) N. Matsuda and S. Biwa: Jpn. J. Appl. Phys. **51** (2012) 07GB14.
17) Y. Udagawa, G. Reim and T. Mihara: Proc. IEEE Ultrasonics Symp., 2012,p 1978.
18) Y. Udagawa and G. Reim: QNDE, R0350410p, 2012.
19) R. C. Wyatt: Non-Destructive Testing, **5** (1972)35.
20) K. Date, Y. Tabata, H. Shimada: Proc. IEEE Ultrasonics Symp., 1987,p. 1093.